Analysis and Reduction of Cross-Modulation Distortion in CDMA Receivers

Vladimir Aparin and Lawrence E. Larson, *Fellow, IEEE*

***Abstract*—The jammer cross modulation (XM) transferred from a transmitter (TX) CDMA leakage by a receiver circuit is analyzed using the Volterra series and statistical theory. The measured "double-hump" XM spectrum is explained based on the CDMA signal statistics derived using the proposed system model of a reverse-link CDMA signal. The analysis shows that the XM distortion is affected by the circuit behavior not only at the jammer and the TX leakage frequencies, but also in the CDMA signal baseband and at the sum and difference of the excitation frequencies. This theory was verified on a 2-GHz Si bipolar junction transistor low-noise amplifier whose out-of-band terminations were optimally tuned to significantly reduce its XM distortion.**

***Index Terms*—Bipolar transistor circuits, code-division multiaccess, cross-modulation (XM) distortion, nonlinear circuits, spectral analysis, statistics, Volterra series.**

I. Introduction

THE continuing miniaturization of CDMA phones makes the receiver (RX) front-end design more challenging. The new generation of antenna duplexers use surface acoustic-wave (SAW) technology and have much smaller size than their predecessors—ceramic duplexers. The isolation between the transmitter (TX) and RX ports of the new duplexers is lower than it used to be and causes a stronger TX leakage to the RX input. This leakage is generally not a problem on its own. However, in the presence of a strong in-band jammer transmitted by a nearby analog base station, the TX leakage modulation is transferred to the jammer by the RX nonlinearities widening the jammer spectrum, as shown in Fig. 1. This widening is called cross modulation (XM). It contaminates the RX channels adjacent to the jammer reducing the RX sensitivity. To comply with the single-tone desensitization requirement of the ANSI/TIA/EIA-98-D Standard [1], CDMA RXs must be designed to be very linear.

To aid the linearization of CDMA RX front ends, the effect of the circuit characteristics on the XM distortion must be understood. This effect can be analyzed using the power series approach [2], [3], which is the tool of popular choice due to its simplicity. However, it is only applicable to memoryless circuits, i.e., circuits with zero reactances and, thus, frequency-independent characteristics. RF circuits do not satisfy this criterion, and require the use of the harmonic-balance circuit envelope or Volterra-series techniques. Though very powerful circuit simulation tools, the harmonic-balance and circuit envelope do not give an insight on how XM is affected by parameters and terminal impedances of an active device. The Volterra-series analysis often gives a closed-form solution for a distortion in a weakly nonlinear circuit showing the contributions of different nonlinearities to the distortion and the effect of out-of-band terminations. The latter can be used to efficiently reduce the circuit distortion [4]–[8].

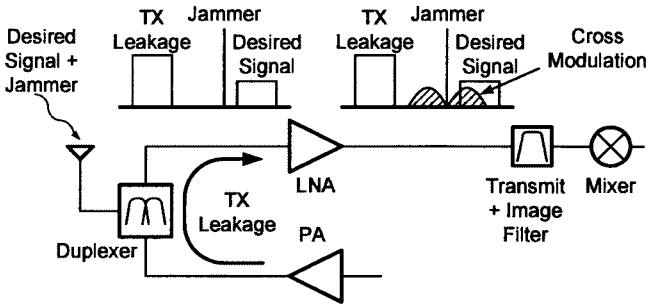

Fig. 1. XM in a CDMA transceiver.

Another challenge of the XM analysis is taking into account the pseudorandom nature of a CDMA signal. The analysis presented in [2] treats the TX CDMA leakage as a narrow-band Gaussian noise (NBGN) yielding the same expression for the total XM power as in [3]. The Gaussian approximation of a CDMA signal is often used in analyzing other types of distortion such as spectral regrowth [9], [10]. The popularity of this approximation is due to the fact that the expansion formulas of the higher order normal moments are well known [11], [12], and they significantly simplify the distortion analysis. However, the NBGN model overestimates the XM distortion and, therefore, requires an empirical fitting of the XM noise in the adjacent RX channel, as in [3]. Nor can it explain a commonly observed XM power drop closer to the jammer center frequency resulting in a "double-hump" spectrum shape. These deficiencies of the Gaussian approximation require a development of a new more accurate model.

Such a model was proposed in [13] and is used here in a more extensive review of the XM distortion in CDMA RXs. Section II gives foundations for this model and uses it to derive the statistical properties of a CDMA signal that are compared to the Gaussian noise properties. Section III uses a Volterra series to analyze the XM of a single-tone jammer in a weakly nonlinear common-emitter circuit. It derives a relationship between the XM distortion and input-referred third-order intercept point (IIP_3). Section IV discusses the dependence of the XM distortion on the circuit out-of-band terminal impedances. This de-

Manuscript received September 8, 2002; revised November 4, 2002.

V. Aparin is with QUALCOMM Inc., San Diego, CA 92121 USA and also with the Department of Electrical Engineering, University of California at San Diego, La Jolla, CA 92093-0407 USA (e-mail: vaparin@qualcomm.com).

L. E. Larson is with the Center for Wireless Communications, University of California at San Diego, La Jolla, CA 92093-0407 USA.

Digital Object Identifier 10.1109/TMTT.2003.810144

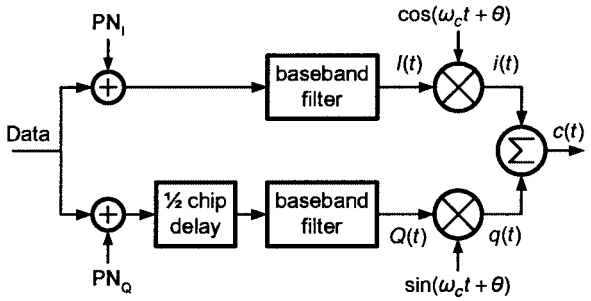

Fig. 2. IS-95 CDMA reverse-link modulator.

pendence was used to efficiently linearize a 2-GHz Si bipolar junction transistor (BJT) low-noise amplifier (LNA) described in Section V. Section VI presents measured data to confirm the theoretical results.

II. Time-Domain Model and Statistical Properties of CDMA Signal

To aid the XM analysis, a CDMA signal will be described here in the time domain according to the IS-95 CDMA reverse-link modulation scheme shown in Fig. 2. The binary-valued transmitted data is first split into the I and Q data sequences and spread by the orthogonal PN codes at the rate $R_s = 1.2288$ Mc/s using a modulo-2 addition. The spreading codes are assumed infinitely long. The Q sequence is delayed by half a PN chip time resulting in offset quadrature phase-shift keying (OQPSK) spreading. After passing the baseband filters, the I and Q sequences become

$$I(t) = \sum_{k=-\infty}^{\infty} i_k h\big(t + (\phi/\pi - k)T_s\big) \tag{1a}$$

$$Q(t) = \sum_{k=-\infty}^{\infty} q_k h\big(t + (\phi/\pi - k + 1/2)T_s\big) \tag{1b}$$

where i_k and q_k are uncorrelated random numbers taking values of ± 1 with equal probability, $h(t)$ is the impulse response of the filters, ϕ is a random phase uniformly distributed in $(0, \pi)$, and T_s is the chip time equal to $1/R_s$.

The IS-95 baseband filter is implemented as a 48-tap finite impulse response (FIR) filter with the impulse and frequency responses shown in Fig. 3. With an acceptable accuracy, it can be modeled as an ideal low-pass filter with the cutoff frequency of $B/2$ and infinite impulse response $h(t) = \mathrm{sinc}(Bt)$, where $\mathrm{sinc}(z) = \sin(\pi z)/(\pi z)$ and $B = 1/T_s = 1.2288$ MHz. The impulse and frequency responses of this brick-wall filter are compared to the IS-95 filter responses in Fig. 3. With this approximation, the filtered I and Q signals are given by

$$I(t) = \sum_{k=-\infty}^{\infty} i_k \mathrm{sinc}(Bt + \phi/\pi - k) \tag{2a}$$

$$Q(t) = \sum_{k=-\infty}^{\infty} q_k \mathrm{sinc}(Bt + \phi/\pi - k + 1/2). \tag{2b}$$

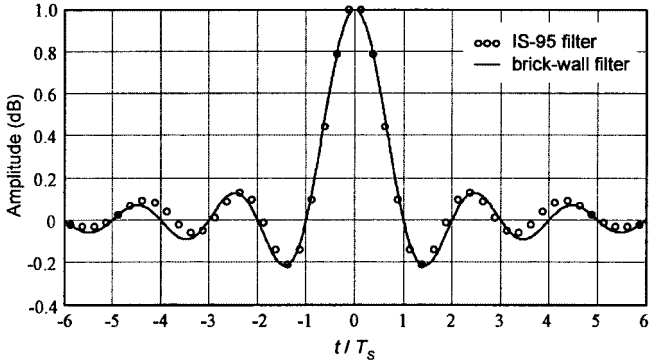

(a)

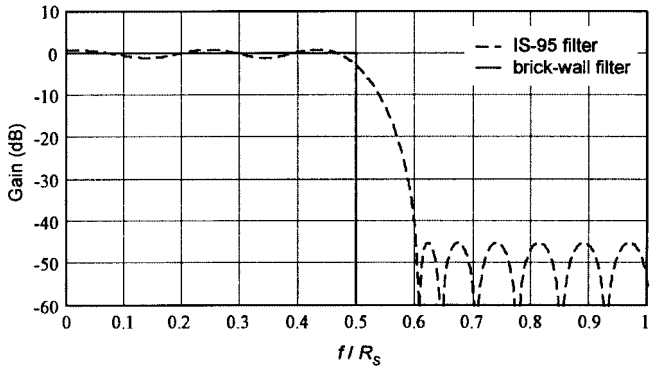

(b)

Fig. 3. Responses of IS-95 and brick-wall filters. (a) Impulse responses. (b) Frequency responses.

After the baseband pulse shaping, the I and Q signals are modulated on two carriers in quadrature and summed producing the transmitted signal

$$c(t) = i(t) + q(t) \tag{3a}$$

where

$$i(t) = \cos(\omega_c t + \theta) \sum_{k=-\infty}^{\infty} i_k \mathrm{sinc}(Bt + \phi/\pi - k) \tag{3b}$$

$$q(t) = \sin(\omega_c t + \theta) \sum_{k=-\infty}^{\infty} q_k \mathrm{sinc}(Bt + \phi/\pi - k + 1/2) \tag{3c}$$

ω_c is the angular frequency of the carriers and θ is their random phase independent of ϕ and uniformly distributed in $(0, 2\pi)$. Equations (3a)–(3c) constitute the time-domain model of a reverse-link CDMA signal with unity variance. In general, this signal can be described as $V_{c,\mathrm{rms}}c(t)$, where $V^2_{c,\mathrm{rms}}$ is its mean-square voltage or variance. A forward-link CDMA signal is quadrature phase-shift key (QPSK) modulated and, for a single active Walsh-coded channel, is also modeled by (3a)–(3c) without 1/2 in the sinc-function argument of (3c).

According to the interpolation formula of the sampling theorem [14], any signal confined to the band $(-B/2, B/2)$ can be accurately represented by an infinite sum of the sinc pulses spaced periodically $1/B$ seconds apart and weighted by the signal samples at the corresponding time instants. Thus, (3a)–(3c) can be viewed as a general time-domain model of

two band-limited signals OQPSK modulated on a carrier with i_k and q_k being their samples. If these samples are normally distributed, (3a)–(3c) describe NBGN. Thus, the important difference between the models of a CDMA signal and NBGN is in the statistical properties of the i_k and q_k samples.

The correlation properties of i_k and q_k for a CDMA signal $c(t)$ and NBGN $n(t)$ are the same and are given by

$$E\{i_k q_l\} = E\{i_k\}E\{q_l\} = 0 \tag{4a}$$

$$E\{i_k i_l\} = E\{q_k q_l\} = \begin{cases} 1, & \text{if } k = l \\ 0, & \text{if } k \neq l \end{cases} \tag{4b}$$

where $E\{\}$ is the statistical average (or expectation). Distortion analysis also requires the knowledge of the nth moments of the i_k and q_k samples. For a CDMA signal

$$E\{i_k^n\} = E\{q_k^n\} = \begin{cases} 0, & \text{if } n \text{ is odd} \\ 1, & \text{if } n \text{ is even} \end{cases} \tag{5}$$

and, for NBGN [11]

$$E\{i_k^n\} = E\{q_k^n\} = \begin{cases} 0, & \text{if } n \text{ is odd} \\ 1 \cdot 3 \cdot 5 \cdots (n-1), & \text{if } n \text{ is even.} \end{cases} \tag{6}$$

Thus, the higher even-order moments of the I and Q samples for NBGN exceed those for a CDMA signal, which causes NBGN to exhibit a stronger distortion.

Since $E\{i_k\} = E\{q_k\} = 0$, both a CDMA signal and NBGN have *zero mean*. Due to the randomness and zero cross-correlation of ϕ and θ, the statistical properties of $i(t)$ and $q(t)$ are time independent. Thus, a CDMA signal and NBGN and their distortions are *stationary* processes under the made assumptions. To shorten the formulas, the time variable t will be set to zero in further derivations without losing accuracy. As shown in Appendix A, $c(t)$ and $n(t)$ have the same autocorrelation function given by

$$R_c(\tau) = R_n(\tau) = \text{sinc}(B\tau)\cos(\omega_c \tau). \tag{7}$$

The Fourier transform of this autocorrelation function yields the following two-sided power spectral density (PSD) function

$$S_c(\omega) = S_n(\omega) = \begin{cases} 1/(2B), & ||\omega| - \omega_c| \leq \pi B \\ 0, & \text{otherwise.} \end{cases} \tag{8}$$

In the remainder of this paper, to shorten expressions for the PSD, only the frequency ranges where it is nonzero will be mentioned.

The characteristic function of a reverse-link CDMA signal is derived in Appendix B and is given by

$$M(v) = \frac{1}{2\pi^2}\int_0^{2\pi} d\theta \int_0^{\pi} d\phi \prod_{k=-\infty}^{\infty} \cos\left[v\cos(\theta)\frac{\sin(\phi)}{\phi - k\pi}\right] \cdot \cos\left[v\sin(\theta)\frac{\cos(\phi)}{\phi - k\pi + \pi/2}\right]. \tag{9}$$

The above integral belongs to a group of sinc-related integrals that do not have analytical solutions according to [15]. It was computed numerically and then, using the inverse Fourier transform (IFT), converted to a probability density function (PDF) that is plotted as a solid line in Fig. 4, where x is the instantaneous voltage and $P(x)$ is its probability. The characteristic function of a QPSK modulated signal such as a single-channel forward-link CDMA signal is the same as (9) with $\pi/2$ omitted and $\cos(\phi)$ replaced with $\sin(\phi)$ in the second brackets. Its PDF obtained by IFT is also plotted in Fig. 4 together with the PDF of NBGN for comparison. As can be seen, the PDFs of OQPSK and QPSK modulated signals significantly differ from the Gaussian PDF and, therefore, the expansion formulas of the higher order joint normal moments used in [2], [9], and [10] as part of the Gaussian approximation cannot be used in analyzing distortions of these signals. The joint moments of a CDMA signal applicable for a power series analysis of distortions up to the third order were derived in closed form in [16].

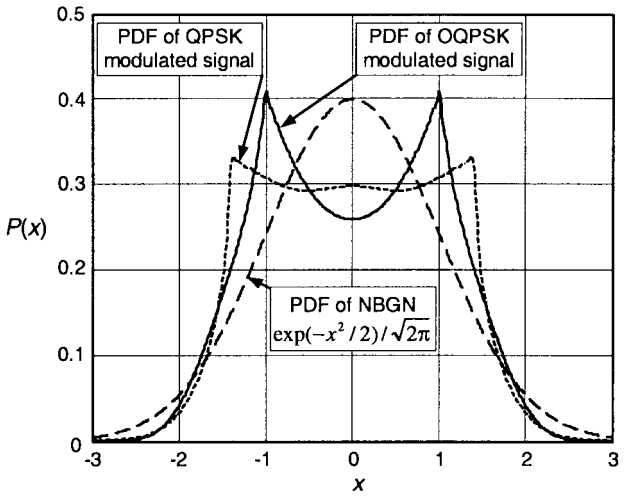

Fig. 4. PDFs of OQPSK and QPSK modulated signals compared to a Gaussian PDF.

III. XM Analysis

Here, we derive an expression for the total XM power generated in the CDMA receive band by a weakly nonlinear circuit. This is accomplished by calculating the Fourier transform of the autocorrelation of the third-order response of the circuit based on a Volterra-series analysis.

Let the input signal $x(t)$ of an RX circuit be

$$x(t) = j(t) + l(t) \tag{10}$$

where $j(t) = V_j\cos(\omega_j t + \psi)$ is a single-tone jammer with a constant amplitude V_j and a random phase ψ uniformly distributed over the interval $(0, 2\pi)$, and $l(t) = V_{c,\text{rms}}c(t)$ is a TX CDMA leakage with a root-mean-square voltage $V_{c,\text{rms}}$ and $c(t)$ defined by (3a). After passing through the circuit, the jammer spectrum is widened by the XM distortion generated by the circuit nonlinearities. The XM distortion acts as an interference to a weak desired signal adjacent to the jammer. Our goal is to find the XM power that falls within the desired signal band. Since the source of XM is the TX leakage, the analysis does not require the presence of the desired signal and, therefore, the latter will be omitted. Only its location relative to the jammer will be considered.

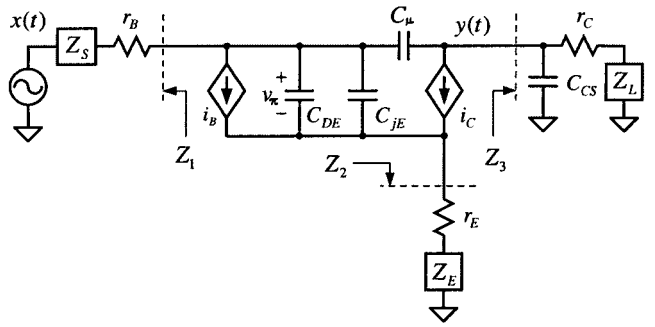

Fig. 5. Equivalent circuit of a common-emitter stage.

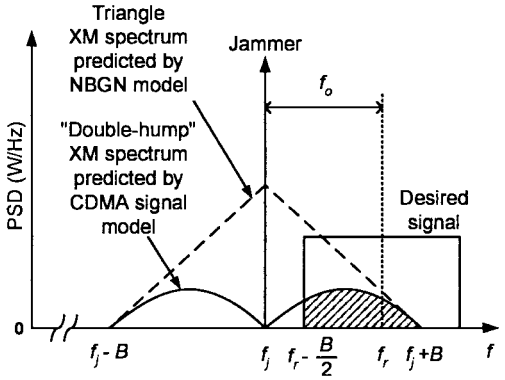

Fig. 6. Spectrum of XM distortion.

In a general case of a circuit with memory, the output signal can be expanded in the following Volterra series [12]:

$$y(t) = \sum_{n=1}^{\infty} y_n(t) \tag{11}$$

where

$$y_n(t) = \int_{-\infty}^{\infty} \cdots \int_{-\infty}^{\infty} b_n(\tau_1, \ldots, \tau_n) \prod_{k=1}^{n} x(t-\tau_k)\, d\tau_k \tag{12}$$

and $b_n(\tau_1, \ldots, \tau_n)$ is the nth-order Volterra kernel describing the circuit's nonlinear impulse response of order n.

The TX modulation is transferred to the jammer by the odd-order nonlinear terms in (11). Terms of order higher than three will be neglected here since most RX front-end circuits operate far below their 1-dB gain compression. The circuit impedances will be assumed frequency independent within $\pm 2\pi B$ around ω_j, ω_c, $\omega_j - \omega_c$, and $\omega_j + \omega_c$.

As shown in Appendix C, the jammer XM is described by the following two-sided spectral density function:

$$S_{\mathrm{XM}}(\omega) = \frac{9V_j^2 V_{c,\mathrm{rms}}^4}{4B} \frac{||\omega| - \omega_j|}{2\pi B} \left(1 - \frac{||\omega| - \omega_j|}{2\pi B}\right) \cdot \left|B_3\big(|\omega| - \omega_j - \omega_c, \omega_c, \omega_j\big)\right|^2 \tag{13}$$

for $||\omega| - \omega_j| < 2\pi B$, where $B_3(\omega_1, \omega_2, \omega_3)$ is the three-dimensional Fourier transform of the Volterra kernel $b_3(\tau_1, \tau_2, \tau_3)$, also known as the third-order nonlinear transfer function. It can be derived using the harmonic input or nonlinear current methods [12]. For a common-emitter stage shown in Fig. 5, $B_3(\omega_1, \omega_2, \omega_3)$ has already been derived and was published in [6], [8], and [17]. The result presented in [6] is more general by including the effect of the base–collector capacitance. Using this result, we get

$$B_3(\omega_1, \omega_2, \omega_3) = B_1(\omega_\Sigma) H(\omega_\Sigma) A_1(\omega_1) A_1(\omega_2) A_1(\omega_3) \cdot \varepsilon(\omega_1 + \omega_2, \omega_1 + \omega_3, \omega_2 + \omega_3) \tag{14}$$

where $B_1(\omega)$ is the linear transfer function (voltage gain) of the stage, $\omega_\Sigma = \omega_1 + \omega_2 + \omega_3$, $H(\omega)$ relates the equivalent input third-order distortion voltage to the third-order distortion response of the i_C nonlinear terms, $A_1(\omega)$ is the linear transfer function of x to v_π,

$$\varepsilon(u, v, w) = g_3 - \frac{2g_2^2}{3}\left[\frac{1}{g_1 + g(u)} + \frac{1}{g_1 + g(v)} + \frac{1}{g_1 + g(w)}\right] \tag{15}$$

$$g(\omega) = \frac{j\omega C_{jE} + \dfrac{1 + j\omega C_\mu \big[Z_1(\omega) + Z_3(\omega)\big]}{Z_1(\omega) + Z_x(\omega)}}{1/\beta + j\omega\tau_F + \dfrac{Z_x(\omega)}{Z_1(\omega) + Z_x(\omega)}} \tag{16}$$

$$Z_x(\omega) = Z_2(\omega) + j\omega C_\mu \big[Z_1(\omega) Z_2(\omega) + Z_1(\omega) Z_3(\omega) + Z_2(\omega) Z_3(\omega)\big] \tag{17}$$

g_n $(n = 1, 2, 3)$ are the $i_c(v_\pi)$ Taylor-series coefficients, C_{jE} is the base–emitter junction capacitance, $C_\mu$is the base–collector junction capacitance, τ_F is the forward transit time, β is the forward dc current gain, and Z_n $(n = 1, 2, 3)$ are the terminal impedances defined in Fig. 5. The third-order nonlinear transfer function of a common-source stage is also described by (14)–(17) with $\tau_F = 0$, $\beta = \infty$, $C_{jE} = C_{GS}$, $C_\mu = C_{GD}$, $r_B = r_G$, $r_E = r_S$, and $r_C = r_D$, where the subscripts G, S, and D stand for gate, source, and drain, respectively.

Substituting (14) into (13), we obtain

$$S_{\mathrm{XM}}(\omega) = \frac{9V_j^2 V_{c,\mathrm{rms}}^4}{4B} \frac{||\omega| - \omega_j|}{2\pi B} \left(1 - \frac{||\omega| - \omega_j|}{2\pi B}\right) \cdot \big|B_1(\omega_j) H(\omega_j) A_1(\omega_j)\big|^2 \big|A_1(\omega_c)\big|^4 \cdot \left|\varepsilon\big(|\omega| - \omega_j, \omega_j - \omega_c, \omega_j + \omega_c\big)\right|^2. \tag{18}$$

If $g(\omega)$ is constant in the CDMA baseband $(0, B)$, the XM spectrum in the linear scale is outlined by two parabolas centered at $f_j - B/2$ and $f_j + B/2$, turned upside down and reaching zero at $f_j - B$, f_j and $f_j + B$, as shown in Fig. 6. This "double-hump" XM spectrum shape is due to the CDMA signal statistics. By contrast, the analysis based on modeling the CDMA signal as NBGN predicts a triangle XM spectrum centered at the jammer frequency [2].

The XM power in the adjacent RX channel is determined by the jammer offset from the channel center frequency ($f_o = f_r -$

f_j) and by the channel filter bandwidth (B). When referred to the source as the available power, it is given by

$$P_{\mathrm{XMU}} = \frac{1}{\pi}\int_{\omega_r-\pi B}^{\omega_j+2\pi B} \frac{S_{\mathrm{XM}}(\omega)}{4\mathrm{Re}\big(Z_S(\omega)\big)\big|B_1(\omega)\big|^2}\,d\omega \qquad (19)$$

where a factor of two is included to take into account the negative frequency spectrum. The letter "U" in the subscript differentiates the XM power in the RX channel above the jammer frequency from that in the channel below f_j (P_{XML}). Assuming that $g(\omega)$ is constant in the frequency range ($\omega_o-\pi B,\ 2\pi B$) that will be denoted as ω_{bb}, we get

$$\begin{aligned} P_{\mathrm{XMU}} = {} & 48P_jP_c^2\mathrm{Re}\,(Z_S(\omega_c))^2\,\frac{f_o}{B}\left(\frac{3}{2}-\frac{f_o}{B}\right)^2 \\ & \cdot\big|H(\omega_j)A_1(\omega_j)\big|^2\big|A_1(\omega_c)\big|^4 \\ & \cdot\big|\varepsilon(\omega_{\mathrm{bb}},\,\omega_j-\omega_c,\,\omega_j+\omega_c)\big|^2 \end{aligned} \qquad (20)$$

where P_j and P_c are the input-referred available jammer and TX leakage powers equal to $V_j^2/[8\mathrm{Re}(Z_S(\omega_j))]$ and $V_{c,\mathrm{rms}}^2/[4\mathrm{Re}(Z_S(\omega_c))]$, respectively. The equation for P_{XML} is the same as (20), but with the minus sign in front of ω_{bb}.

XM distortion is often estimated from IIP_3 because the latter is easier to simulate or measure. The RX IIP_3 is usually evaluated in the RX band. If the two excitation tones are at ω_j and $\omega_j+\Delta\omega$, IIP_3 for the upper-side intermodulation term is given in [6] as

$$\mathrm{IIP}_{3U} = \frac{1}{6\mathrm{Re}\big(Z_S(\omega_j)\big)\big|H(\omega_j)\|A_1(\omega_j)\big|^3\varepsilon(\Delta\omega,\,\Delta\omega,\,2\omega_j)}. \qquad (21)$$

Solving for $|H(\omega_j)|$ in (21) and substituting it to (20) gives

$$\begin{aligned} P_{\mathrm{XMU}} = {} & \frac{4P_jP_c^2}{3\mathrm{IIP}_{3U}^2}\,\frac{f_o}{B}\left(\frac{3}{2}-\frac{f_o}{B}\right)^2\left[\frac{\mathrm{Re}\big(Z_S(\omega_c)\big)}{\mathrm{Re}\big(Z_S(\omega_j)\big)}\right]^2 \\ & \cdot\left|\frac{A_1(\omega_c)}{A_1(\omega_j)}\right|^4\left|\frac{\varepsilon(\omega_{\mathrm{bb}},\,\omega_j-\omega_c,\,\omega_j+\omega_c)}{\varepsilon(\Delta\omega,\,\Delta\omega,\,2\omega_j)}\right|^2. \end{aligned} \qquad (22)$$

This formula shows that the relationship between XM and IIP_3 is frequency dependent and, therefore, IIP_3 is not always a good estimate of XM. Neglecting this frequency dependence and substituting $f_o = 0.9$ MHz for cellular RXs and $f_o = 1.25$ MHz for personal communications system (PCS) RXs, we get

$$P_{\mathrm{XM}}\ [\mathrm{dBm}] = P_j + 2P_c - 2\mathrm{IIP}_3 - \begin{cases} 2.4, & \text{cellular RX} \\ 5.0, & \text{PCS RX} \end{cases} \qquad (23)$$

where "U" in the subscripts of P_{XM} and IIP_3 was omitted to reflect the symmetry in the XM and intermodulation distortions in frequency-independent circuits. Equation (23) predicts 3.1 and 1.7 dB less XM power in a cellular and PCS channels, respectively, than a similar formula derived using the Gaussian approximation of the CDMA signal [2].

IV. Effect of Out-of-Band Terminations on XM Distortion

Equation (18) provides an insight into how an amplifier can be linearized. It shows that the XM distortion depends on the circuit *in-band* impedances, i.e., those at ω_j and ω_c (fundamental frequencies), and *out-of-band* impedances, i.e., those in the CDMA baseband and at $\omega_j-\omega_c$ and $\omega_j+\omega_c$ (second-order mixing frequencies). The dependence on the out-of-band impedances is introduced by ε that describes the distortion contribution of the second-order nonlinearity of the device transconductance g_2. Even though the XM is the odd-order distortion, the second-order nonlinearity still contributes to it by first generating second-order responses and then, after they are fed back to the input, mixing them with the fundamental excitations. In a common-emitter stage, the feedback paths are provided by the emitter-degeneration network, the base–emitter and base–collector junctions. If the operating frequency is low enough to neglect the effect of the feedback capacitances at and below the second harmonic frequency, in the absence of the emitter degeneration, $|\varepsilon| \cong |g_3|$.

Examination of (16) and (17) shows that, if the terminal impedances Z_1, Z_2, and Z_3 have positive real parts, which is usually the case, $\mathrm{Re}(g(\omega))$ is also positive. Therefore, for RF amplifiers, $|\varepsilon|$ can be made less than $|g_3|$ provided that g_3 is positive, i.e., the device exhibits gain expansion for small signals. This is exactly the behavior of BJTs. Their out-of-band terminal impedances can be selectively tuned so that the XM responses of the self-interacting second-order nonlinearity cancel those of the third-order nonlinearity according to (15). The resulting XM distortion can theoretically be zero regardless of the input power.

The optimum Z_S and Z_L in the CDMA baseband and at $\omega_j-\omega_c$ and $\omega_j+\omega_c$ are found by setting ε to zero. To cancel the XM distortion within the RX channel adjacent to the jammer for different ω_c and ω_j,[1] $g(\omega)$ that is responsible for the frequency dependence of ε should be constant in the corresponding ranges of the second-order mixing frequencies, i.e.,

$$g(\omega_{\mathrm{bb}}) = 1/r, \qquad \text{where } \omega_o-\pi B < \omega_{\mathrm{bb}} < 2\pi B \qquad (24a)$$

$$g(\omega_j-\omega_c) = 1/p \qquad (24b)$$

$$g(\omega_j+\omega_c) = \left(\frac{3g_3}{2g_2^2} - \frac{r}{1+g_1r} - \frac{p}{1+g_1p}\right)^{-1} - g_1 \qquad (24c)$$

where r and p are some constants in units of Ω, and the right-hand side of (24c) is derived to make ε zero. Equations (24a)–(24c) are underdetermined and, therefore, have many solutions for optimum out-of-band Z_S and Z_L.

If $g(-\omega_{\mathrm{bb}}) = g(\omega_{\mathrm{bb}})$, the baseband second-order distortion response from the TX leakage modulates only the jammer amplitude resulting in a symmetrical XM spectrum ($P_{\mathrm{XML}} = P_{\mathrm{XMU}}$). If, on the other hand, $g(-\omega_{\mathrm{bb}}) \neq g(\omega_{\mathrm{bb}})$, the baseband response modulates not only the amplitude, but also the phase of the jammer. The resulting XM spectrum will have asymmetry,

[1]Since the offset of the RX channel from the TX channel $f_r - f_c$ is fixed, as defined in the ANSI/TIA/EIA-98-D Standard, f_j is equal to $f_c + 45$ MHz $\pm f_o$ for the cellular band and $f_c + 80$ MHz $\pm f_o$ for the PCS band

i.e., $P_{\mathrm{XML}} \neq P_{\mathrm{XMU}}$, and the XM noise cannot be cancelled on both sides of the jammer simultaneously. Since $g(-\omega_{\mathrm{bb}})$ is conjugate to $g(\omega_{\mathrm{bb}})$, to avoid the XM spectrum asymmetry, the bias circuit should be designed so that $\mathrm{Im}(g(\omega_{\mathrm{bb}})) \approx 0$, i.e., its reactances should be minimized in the CDMA baseband. Therefore, r in (24a) and (24c) should be real.

The out-of-band load impedance affects XM due to the feedback through C_μ. For a typical narrow-band RF circuit, Z_L is much smaller than the impedance of C_μ in the CDMA baseband and at $\omega_j - \omega_c$. Thus, the feedback through C_μ and the effect of Z_L at these frequencies can be neglected. Furthermore, by making $p = r$, (24a) and (24b) can be combined into a single equation for the optimum source impedance in the frequency range $(\omega_o - \pi B, \omega_j - \omega_c)$. For an inductively degenerated common-emitter stage with $Z_2(\omega) = r_2 + j\omega L_2$, the solution of this equation is very accurately approximated by

$$Z_{S,\,\mathrm{opt}}(\omega) \cong \beta(r - r_2) - r_B - j\omega\beta\big[L_2 + \beta(\tau_F - rC_{jE})(r - r_2)\big]. \quad (25)$$

The optimum source and load impedances at $\omega_j + \omega_c$ are found from (24c) with $p = r$. If the BJT operates below the high-injection region and above the low-current nonideal region

$$g_1 = \frac{I_C}{V_T} \quad g_2 = \frac{I_C}{2V_T^2} \quad g_3 = \frac{I_C}{6V_T^3} \quad (26)$$

and $3g_3/(2g_2^2) = 1/g_1$. In this case, (24c) simplifies to

$$g(\omega_j + \omega_c) = \frac{2g_1}{\dfrac{1}{g_1 r} - 1}. \quad (27)$$

Three important observations can be made from (25) and (27) as follows.

1) For a given value of r, the optimum source and load impedances at $\omega_j + \omega_c$ depends upon the BJT small-signal transconductance g_1 that is proportional to the collector dc current. This dependence is undesirable and can be minimized if r is chosen much smaller than $1/g_1$.
2) If $r < r_2 + r_B/\beta$, $\mathrm{Re}(Z_{S,\,\mathrm{opt}}(\omega))$ in the frequency range $(\omega_o - \pi B, \omega_j - \omega_c)$ is negative and cannot be implemented without making the circuit unstable. On the other hand, choosing r relatively large may force the solutions to (27) to have negative real parts, which is not desirable either.
3) The optimum source impedance at low frequencies strongly depends on β that varies by over 50% over process and temperature for a typical bipolar process. This dependence may cause XM of an optimally terminated circuit to vary by several decibels.

The presented analysis of the distortion cancellation is based on zeroing B_3. The contributions of the fifth-order and higher odd-order terms of $y(t)$ were neglected. Generally, these terms are not cancelled by tuning Z_S and Z_L at the out-of-band frequencies that affect only B_3.

It should also be noted that, according to (20) and (21), the out-of-band frequencies affecting XM are not the same as those affecting IIP_3. Therefore, tuning the out-of-band Z_S and Z_L for the highest IIP_3 may not necessarily lead to the lowest XM.

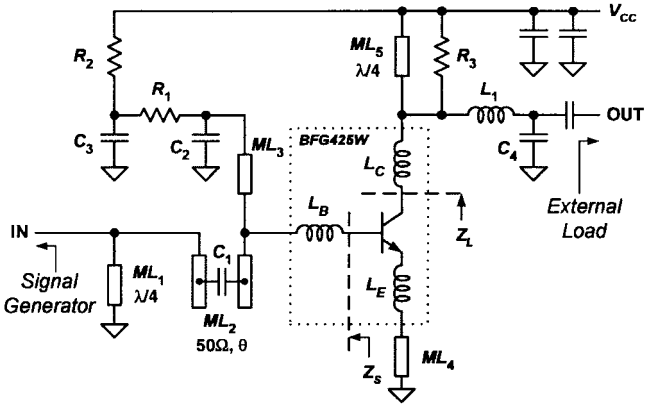

Fig. 7. Schematic diagram of the 2-GHz LNA.

On a final note, if one attempts to use the out-of-band tuning of terminal impedances for a distortion cancellation in a MOSFET biased in the strong-inversion region, the desired result will not be achieved since g_3 is usually negative in this region. The device must be biased in the subthreshold or weak-inversion region where $g_3 > 0$ and, thus, $|\varepsilon|$ can be reduced below $|g_3|$ according to (15).

V. Low-Distortion 2-GHz LNA Design

A schematic diagram of the designed 2-GHz LNA is shown in Fig. 7, where the dashed box marks the boundaries of a discrete bipolar transistor, and the inductances inside the box (L_B, L_E, and L_C) model the bond wires. The components outside the dashed box are implemented on a printed circuit (PC) board. The discrete transistor is biased at a 5-mA collector current from a 2.7-V supply. The operating frequency of the LNA was chosen outside the commercial frequency bands just to demonstrate the developed XM distortion theory. In a practical application, the impedances of an external source and load outside the operating frequency range are not well defined. To avoid the XM dependence on these impedances, they are decoupled from the transistor terminals by the shunt $\lambda/4$ microstrip lines ML_1 and ML_5. These lines are almost open circuits around 2 GHz and do not affect the LNA in-band performance. For simplicity, only the out-of-band source impedance is optimally tuned for low XM. The out-of-band load impedance is fixed by ML_5 such that $Z_L(\omega_j + \omega_c) \approx j(\omega_j + \omega_c)L_C$ and $Z_L(\omega_{\mathrm{bb}}) \approx Z_L(\omega_j - \omega_c) \approx 0\ \Omega$.

With the signal generator shorted to ground at $\omega_j + \omega_c$, a well-controlled nonzero real part of $Z_S(\omega_j + \omega_c)$ can only be produced by a resistor in the input matching network. We found that this resistor cannot be well isolated from the LNA input in a wide-enough frequency range around 2 GHz and, as a result, it degrades the LNA NF. To avoid the use of this resistor, the allowed values of $Z_S(\omega_j + \omega_c)$ were limited to those with the real part close to zero. For given $Z_L(\omega_j + \omega_c)$, this restriction allowed us to solve (27) for r and optimum $\mathrm{Im}(Z_S(\omega_j + \omega_c))$. Once r was defined, $Z_{S,\,\mathrm{opt}}$ in the $(\omega_o - \pi B, \omega_j - \omega_c)$ range was found from (25). $\mathrm{Im}(Z_{S,\,\mathrm{opt}}(\omega))/\omega$ turned out to be a negative constant in this frequency range.

The input matching network is designed to match the LNA input to 50 Ω around 2 GHz and to optimally terminate it at

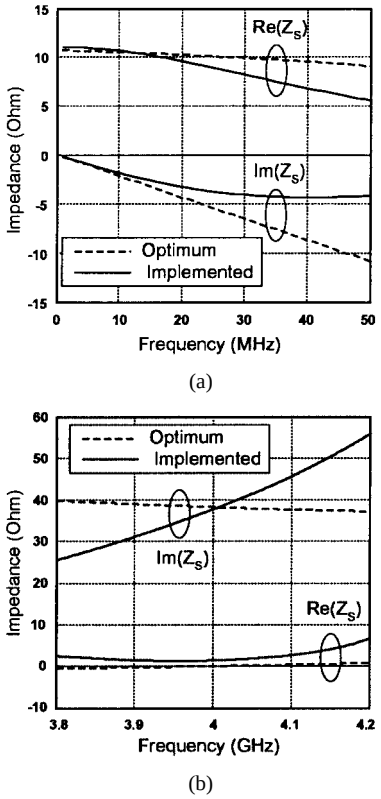

Fig. 8. Implemented Z_S versus desired $Z_{S,\,\mathrm{opt}}$. (a) Near dc. (b) Near $f_j + f_c$.

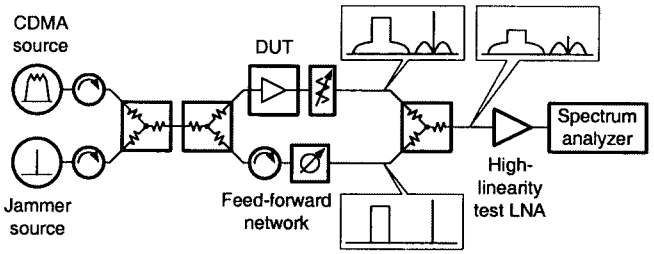

Fig. 9. Test setup for measuring XM distortion.

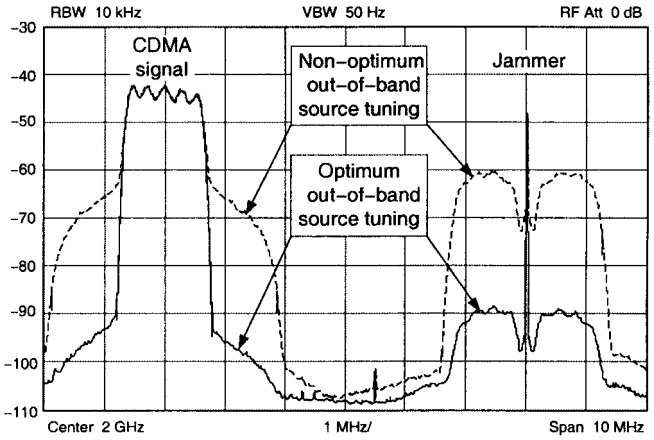

Fig. 10. Measured output spectra ($P_j = P_c = -23$ dBm).

$f_j + f_c$ of 4 GHz in the CDMA baseband and at $f_j - f_c$ up to 50 MHz. ML_3 ac grounded by C_2 is used for in-band matching. Z_S in the CDMA baseband and at $f_j - f_c$ is set by tunable R_1 in parallel with C_2. The time constant of this *RC* network is selected much smaller than $1/(\omega_j - \omega_c)$ such that $Z_S(\omega) \approx R_1 - j\omega C_2 R_1^2$ in the $(\omega_o - \pi B,\, \omega_j - \omega_c)$ range, where $-C_2R_1^2$ is equal to the desired negative constant $\mathrm{Im}(Z_{S,\,\mathrm{opt}}(\omega))/\omega$. The value of C_2 is still large enough to provide a good ac ground for ML_3 and to isolate R_1 from the LNA input at 2 GHz. C_3 is the ac ground for R_1. R_2 is used to set the BJT dc-bias current. $Z_S(\omega_j + \omega_c)$ is defined by tunable ML_2 in parallel with ML_3. ML_2 is tuned by sliding the dc blocking capacitor C_1 along the parallel portions of ML_2. Since the characteristic impedance of ML_2 is 50 Ω and ML_1 is an open circuit around 2 GHz, the ML_2 tuning does not affect the LNA in-band input match. The implemented source impedance is plotted as a function of frequency and compared to the desired $Z_{S,\,\mathrm{opt}}$ predicted by the theory in Fig. 8.

ML_4 in series with L_E is used to bring the conjugate input impedance of the transistor closer to the source impedance needed for the minimum noise figure (NF). L_1 and C_4 form the output matching network. R_3 is used for LNA stabilization.

VI. Measured Results

Measuring the XM distortion is complicated by the somewhat high noise floor of a CDMA source, the phase noise of a jammer source, and the distortion introduced by a spectrum analyzer. Fig. 9 shows the test setup developed to overcome these difficulties. The combined CDMA and jammer signals are applied to the DUT input and subtracted from its output. The variable attenuator connected to the DUT output and the phase delay of the feed-forward network are tuned to cancel the jammer and the noise from the sources around it. The jammer cancellation allows the use of a high-linearity test LNA to bring the DUT XM response above the spectrum analyzer noise floor without additional XM distortion in the test LNA and the spectrum analyzer. The feed-forward network should be well isolated from the DUT signal path to prevent the XM distortion produced at the DUT input from coupling to the output through the feed-forward network and to prevent the DUT output signal from coupling back to the input.

Fig. 10 shows two overlapped output spectra of the LNA driven by a jammer with $P_j = -23$ dBm and a 1.23-MHz-wide OQPSK CDMA signal with $P_c = -23$ dBm. The solid line is the output spectrum with the source impedance tuned according to Fig. 8, and the dashed line is the output spectrum of the same LNA with $R_1 = 10$ kΩ and R_2 adjusted such that the dc current is the same in both cases. As can be seen, the optimum out-of-band source tuning reduces the XM distortion by almost 30 dB for the given power levels. It also significantly reduces the spectral regrowth of the CDMA signal. The measured XM spectrum has the "double-hump" shape, as predicted theoretically.

Fig. 11 shows the dependence of the output XM power ($P_{\mathrm{XM\_OUT}}$) on the input power of the jammer and the CDMA signal. $P_{\mathrm{XM\_OUT}}$ was measured 600 kHz away from the jammer in a 10-kHz band. With a nonoptimum out-of-band source impedance, $P_{\mathrm{XM\_OUT}}$ varies by 1 dB per 1 dB of the jammer power and by 2 dB per 1 dB of the CDMA power at low power levels. These slopes are due to the dominating third-order nonlinearity. The described optimum out-of-band

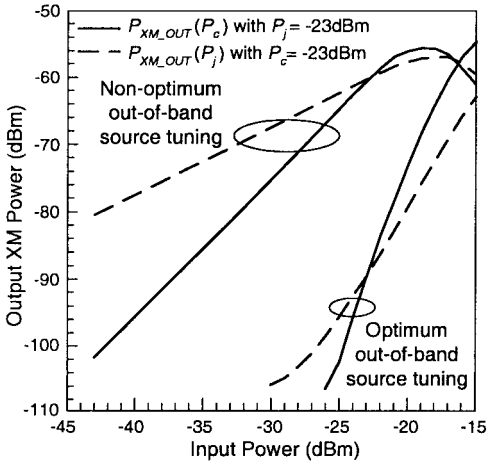

Fig. 11. Output XM power ($P_{\mathrm{XM\_OUT}}$) versus jammer power (P_j) and total CDMA signal power (P_c).

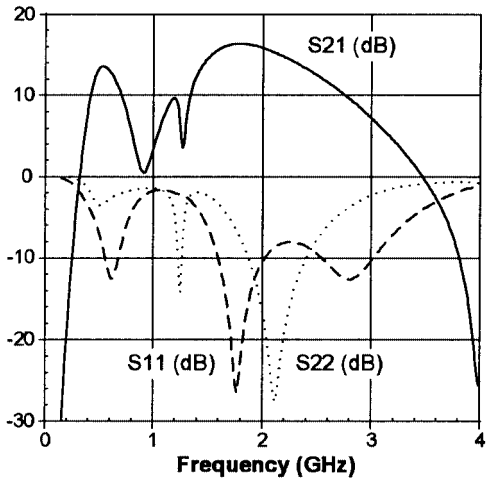

Fig. 12. Measured S-parameters versus frequency.

source tuning cancels this nonlinearity, and the resulting XM distortion is produced by higher odd-order nonlinearities. That is why the slopes of the XM power in this case are steeper.

The out-of-band source tuning did not affect the in-band gain, NF, and input return loss of the LNA. Their measured values at 2 GHz are 16, 1.7, and -10 dB, respectively. The S-parameter plot is shown in Fig. 12. The LNA IIP_3 measured as a function of frequency and the source impedance is reported in [6].

VII. Conclusions

We have shown that a commonly used Gaussian approximation of a CDMA signal fails to predict the XM accurately. The proposed system model of a CDMA signal showed that its statistical properties differ from those of NBGN and are responsible for the measured "double-hump" XM spectrum shape. The Volterra-series analysis demonstrated that the XM is affected by the circuit behavior not only at the jammer and TX leakage frequencies, but also in the CDMA signal baseband and at the sum and difference of the excitation frequencies. This is a larger set of frequencies than the one affecting IIP_3. As a result, the relation between XM and IIP_3 is frequency dependent, and, therefore, IIP_3 is not always a good estimate of XM. The effect of the out-of-band circuit impedances on XM was investigated on an LNA that showed a significant XM reduction when its input matching circuit was optimally tuned outside the excitation frequency bands. The measured XM power was not zero, as predicted by the theory, because of the contribution of the fifth-order and higher odd-order LNA nonlinearities to XM that were ignored in the analysis.

Appendix A

In this section, the autocorrelation function of a reverse-link CDMA signal and NBGN is derived.

For both signals, the autocorrelation of the in-phase component $i(t)$ defined by (3b) is

$$\begin{aligned} R_i(\tau) &= E\{i(0)i(\tau)\} \\ &= E_\theta\{\cos(\theta)\cos(\omega_c\tau+\theta)\} \\ &\quad \cdot E_\phi\left\{\sum_{k=-\infty}^{\infty}\sum_{l=-\infty}^{\infty} E\{i_k i_l\}\cdot \mathrm{sinc}(\phi/\pi-k)\right. \\ &\quad \left.\cdot\mathrm{sinc}(B\tau+\phi/\pi-l)\right\} \end{aligned} \tag{28}$$

where $E_\theta\{\,\}$ and $E_\phi\{\,\}$ are the averages over θ and ϕ, respectively. Since i_k and i_l are uncorrelated for $k \neq l$, only the summation terms with $k = l$ will be nonzero and weighted by $E\{i_k^2\} = 1$. Using the following identity [14]:

$$\sum_{k=-\infty}^{\infty}\mathrm{sinc}(\phi/\pi-k)\mathrm{sinc}(B\tau+\phi/\pi-k) = \mathrm{sinc}(B\tau) \tag{29}$$

we get

$$R_i(\tau) = 1/2\cos(\omega_c\tau)\mathrm{sinc}(B\tau). \tag{30a}$$

Similarly, for the quadrature component $q(t)$ of both signals

$$R_q(\tau) = 1/2\cos(\omega_c\tau)\mathrm{sinc}(B\tau). \tag{30b}$$

The cross-correlation between $i(t)$ and $q(t)$ is zero because their samples are not correlated. Thus, the autocorrelation function of $c(t)$ and $n(t)$ is

$$\begin{aligned} R_c(\tau) &= R_n(\tau) \\ &= E\Big\{[i(0)+q(0)][i(\tau)+q(\tau)]\Big\} \\ &= R_i(\tau)+R_q(\tau) \\ &= \cos(\omega_c\tau)\mathrm{sinc}(B\tau). \end{aligned} \tag{31}$$

Appendix B

In this section, the characteristic function of a reverse-link CDMA signal is derived. By definition [11], this function is

$$\begin{aligned} M(v) &= E\Big\{e^{jvc(t)}\Big\} \\ &= E\Big\{e^{jvi(t)}e^{jvq(t)}\Big\} \\ &= \frac{1}{2\pi^2}\int_0^{2\pi}d\theta\int_0^{\pi}d\phi E_i\Big\{e^{jvi(t)}\Big\}E_q\Big\{e^{jvq(t)}\Big\} \end{aligned} \tag{32}$$

where $E_i\{\,\}$ and $E_q\{\,\}$ are the statistical averages over i_k and q_k samples, respectively. Setting t equal to zero, we get

$$\begin{aligned}
&E_i\Big\{e^{jvi(0)}\Big\} \\
&\quad= E_i\left\{\exp\left[jv\cos(\theta)\sum_{k=-\infty}^{\infty} i_k \mathrm{sinc}(\phi/\pi-k)\right]\right\} \\
&\quad= \prod_{k=-\infty}^{\infty} E_i\Big\{\exp\left[jv\cos(\theta) i_k \mathrm{sinc}(\phi/\pi-k)\right]\Big\} \\
&\quad= \prod_{k=-\infty}^{\infty}\left\{\frac{1}{2}\exp\left[jv\cos(\theta)(-1)\mathrm{sinc}(\phi/\pi-k)\right]\right. \\
&\qquad\qquad \left.+\frac{1}{2}\exp\left[jv\cos(\theta)(+1)\mathrm{sinc}(\phi/\pi-k)\right]\right\} \\
&\quad= \prod_{k=-\infty}^{\infty}\cos\left[v\cos(\theta)\mathrm{sinc}(\phi/\pi-k)\right]. \qquad (33)
\end{aligned}$$

Similarly,

$$E_q\{e^{jvq(0)}\} = \prod_{k=-\infty}^{\infty}\cos\left[v\sin(\theta)\mathrm{sinc}(\phi/\pi-k+1/2)\right]. \qquad (34)$$

Thus, the characteristic function of the CDMA signal is

$$\begin{aligned}
M(v) = \frac{1}{2\pi^2}\int_0^{2\pi} d\theta \int_0^{\pi} d\phi \prod_{k=-\infty}^{\infty}\cos\left[v\cos(\theta)\frac{\sin(\phi)}{\phi-k\pi}\right] \\
\cdot\cos\left[v\sin(\theta)\frac{\cos(\phi)}{\phi-k\pi+\pi/2}\right] \qquad (35)
\end{aligned}$$

where the sinc function was replaced by its definition and simplified.

Appendix C

In this section, the autocorrelation and spectral density functions of the XM distortion are derived.

The autocorrelation function of the third-order term in the Volterra-series expansion of the output signal (11) is

$$\begin{aligned}
R_{y_3}(\tau) &= E\{y_3(t)y_3(t+\tau)\} \\
&= \int_{-\infty}^{\infty}\cdots\int_{-\infty}^{\infty} b_3(\tau_1,\tau_2,\tau_3)b_3(\tau_4,\tau_5,\tau_6) \\
&\quad\cdot R_{xxx}(\tau_1,\ldots,\tau_6)\prod_{k=1}^{6} d\tau_k \qquad (36)
\end{aligned}$$

where

$$R_{xxx}(\tau_1,\ldots,\tau_6) = E\left\{\prod_{l=1}^{3} x(t-\tau_l)x(t+\tau-\tau_{3+l})\right\}. \qquad (37)$$

Interchanging the order of integration and expectation operators in (36) can be easily justified [11]. Replacing $x(t)$ in (37) with $j(t)+V_{c,\mathrm{rms}}c(t)$ splits R_{xxx} into four types of terms as follows:

$$R_{xxx} = R_{jjj} + R_{ccc} + R_{jjc} + R_{jcc} \qquad (38)$$

where the first type is due to intermodulation of the jammer with itself, the second type is due to intermodulation of the CDMA signal with itself, and the last two types are due to intermodulation of the jammer with the CDMA signal. Only the jcc-type terms relate to XM. There are 15 of them. Due to the symmetry of the Volterra kernels [12] (neither permutations of τ_1, τ_2, and τ_3, nor permutations of τ_4, τ_5, and τ_6 change the final result), the jcc terms can be collected into two groups of identical terms as follows:

$$\begin{aligned}
R_{jcc} &= 6V_{c,\mathrm{rms}}^4 V_j^2\cos\left[\omega_j(\tau_1-\tau_2)\right]/2 \\
&\quad\cdot E\{c(-\tau_3)c(\tau-\tau_4)c(\tau-\tau_5)c(\tau-\tau_6)\} \\
&\quad+ 9V_{c,\mathrm{rms}}^4 V_j^2\cos\left[\omega_j(\tau_1-\tau_4+\tau)\right]/2 \\
&\quad\cdot E\{c(-\tau_2)c(-\tau_3)c(\tau-\tau_5)c(\tau-\tau_6)\} \qquad (39)
\end{aligned}$$

where t was set to zero for simplicity. It can be shown that only the last nine terms in (39) contribute to XM. Replacing R_{xxx} in (36) with these nine terms and the Volterra kernels with their three-dimensional Fourier transforms, we get

$$\begin{aligned}
R_{\mathrm{XM}}(\tau) &= \frac{9V_j^2V_{c,\mathrm{rms}}^4}{2(2\pi)^6}\int_{-\infty}^{\infty}\cdots\int_{-\infty}^{\infty} B_3(\omega_1,\omega_2,\omega_3) \\
&\quad\cdot B_3(\omega_4,\omega_5,\omega_6)\prod_{k=1}^{6} e^{j\omega_k\tau_k}\,d\omega_k \\
&\quad\cdot\int_{-\infty}^{\infty}\cdots\int_{-\infty}^{\infty}\cos\left[\omega_j(\tau_1-\tau_4+\tau)\right] \\
&\quad\cdot E\{c(-\tau_2)c(-\tau_3)c(\tau-\tau_5)c(\tau-\tau_6)\}\prod_{k=1}^{6} d\tau_k. \qquad (40)
\end{aligned}$$

Using the following result:

$$\begin{aligned}
&\int_{-\infty}^{\infty}\int_{-\infty}^{\infty}\cos\left[\omega_j(\tau_1-\tau_4+\tau)\right]e^{j\omega_1\tau_1}e^{j\omega_4\tau_4}\,d\tau_1\,d\tau_4 \\
&\quad= 2\pi^2\Big[\delta(\omega_j+\omega_1)\delta(\omega_j-\omega_4)e^{j\omega_j\tau} \\
&\qquad+\delta(\omega_j-\omega_1)\delta(\omega_j+\omega_4)e^{-j\omega_j\tau}\Big] \qquad (41)
\end{aligned}$$

and the sifting property of the delta function, (40) can be simplified to

$$\begin{aligned}
R_{\mathrm{XM}}(\tau) &= \frac{9V_j^2V_{c,\mathrm{rms}}^4}{4(2\pi)^4}\int_{-\infty}^{\infty}\cdots\int_{-\infty}^{\infty} d\omega_2\,d\omega_3\,d\omega_5\,d\omega_6 \\
&\quad\cdot\Big[B_3(-\omega_j,\omega_2,\omega_3)B_3(\omega_j,\omega_5,\omega_6)e^{j\omega_j\tau} \\
&\qquad+B_3(\omega_j,\omega_2,\omega_3)B_3(-\omega_j,\omega_5,\omega_6)e^{-j\omega_j\tau}\Big] \\
&\quad\cdot\int_{-\infty}^{\infty}\cdots\int_{-\infty}^{\infty} d\tau_2\,d\tau_3\,d\tau_5\,d\tau_6 \\
&\quad\cdot e^{j\omega_2\tau_2}e^{j\omega_3\tau_3}e^{j\omega_5\tau_5}e^{j\omega_6\tau_6} \\
&\quad\cdot E\{c(-\tau_2)c(-\tau_3)c(\tau-\tau_5)c(\tau-\tau_6)\}. \qquad (42)
\end{aligned}$$

The statistical average of the product of the CDMA signals can be evaluated as follows:

$$\begin{aligned}E\left\{c^2c^3c^5c^6\right\} &= E\left\{\left(i^2+q^2\right)\left(i^3+q^3\right)\left(i^5+q^5\right)\left(i^6+q^6\right)\right\}\\ &= E\Big\{i^2i^3i^5i^6+q^2q^3q^5q^6+i^2i^3q^5q^6\\ &\quad+i^2i^5q^3q^6+i^2i^6q^3q^5+i^3i^5q^2q^6\\ &\quad+i^3i^6q^2q^5+i^5i^6q^2q^3\Big\}\end{aligned}\tag{43}$$

where c, i, and q stand for $c(t)$, $i(t)$, and $q(t)$ given by (3a)–(3c), respectively, and superscripts 2, 3, 5, and 6 indicate that the corresponding signals are functions of $-\tau_2$, $-\tau_3$, $\tau-\tau_5$, and $\tau-\tau_6$, respectively. The products with an odd number of i^n or q^n multiplicands were omitted in (43) because their averages are zero according to (4a).

Let

$$p_k(t) = \operatorname{sinc}(Bt+\phi/\pi-k)\cos(\omega_c t+\theta)\tag{44a}$$

$$s_k(t) = \operatorname{sinc}(Bt+\phi/\pi-k+1/2)\sin(\omega_c t+\theta)\tag{44b}$$

$\hat{p}_k(t)=i_kp_k(t)$ and $\hat{s}_k(t)=q_ks_k(t)$ where, as before, i_k and q_k are independent random numbers $\in\{-1,+1\}$. Equations (3b) and (3c) can then be rewritten as

$$i(t)=\sum_{k=-\infty}^{\infty}\hat{p}_k(t)=\sum_{k=-\infty}^{\infty}i_kp_k(t)\tag{45a}$$

$$q(t)=\sum_{k=-\infty}^{\infty}\hat{s}_k(t)=\sum_{k=-\infty}^{\infty}q_ks_k(t).\tag{45b}$$

Substituting these definitions into (43), we get

$$\begin{aligned}E\{c^2c^3c^5c^6\} = E\Bigg\{&\sum_{k,l,m,n}\hat{p}_k^2\hat{p}_l^3\hat{p}_m^5\hat{p}_n^6+\hat{s}_k^2\hat{s}_l^3\hat{s}_m^5\hat{s}_n^6\\ &\cdot\hat{p}_k^2\hat{p}_l^3\hat{s}_m^5\hat{s}_n^6+\hat{p}_k^2\hat{p}_l^5\hat{s}_m^3\hat{s}_n^6\\ &\cdot\hat{p}_k^2\hat{p}_l^6\hat{s}_m^3\hat{s}_n^5+\hat{p}_k^3\hat{p}_l^5\hat{s}_m^2\hat{s}_n^6\\ &\cdot\hat{p}_k^3\hat{p}_l^6\hat{s}_m^2\hat{s}_n^5+\hat{p}_k^5\hat{p}_l^6\hat{s}_m^2\hat{s}_n^3\Bigg\}\end{aligned}\tag{46}$$

where the meaning of the superscripts is the same as in (43) and the summation operator with four indexes denotes four independent infinite sums over these indexes. Using the correlation properties (4a), it can be shown that

$$\begin{aligned}E&\left\{\sum_{k,l,m,n}\hat{p}_k^2\hat{p}_l^3\hat{p}_m^5\hat{p}_n^6\right\}\\ &= E_{\theta,\phi}\left\{\sum_{k,l}p_k^2p_k^3p_l^5p_l^6+p_k^2p_k^5p_l^3p_l^6\right.\\ &\qquad\left.+p_k^2p_k^6p_l^3p_l^5-2p_k^2p_k^3p_k^5p_k^6\right\}.\end{aligned}\tag{47}$$

The correction term $-2p_k^2p_k^3p_k^5p_k^6$ appears on the right-hand side of the above equation because it was counted three times in the first three terms. Since the fourth-order moment of i_k is one according to (5), the correction had to be applied. It is interesting to note that, if i_k and q_k were Gaussian noise samples, their fourth-order moment would be three according to (6) and no correction would be needed.

Due to the symmetry of the Volterra kernels, permutations of τ_2 and τ_3 or permutations of τ_5 and τ_6 should not change the final result. Therefore, the second and third summands on the right-hand side of (47) can be combined reducing (47) to

$$\begin{aligned}E&\left\{\sum_{k,l,m,n}\hat{p}_k^2\hat{p}_l^3\hat{p}_m^5\hat{p}_n^6\right\}\\ &= E_{\theta,\phi}\left\{\sum_{k,l}p_k^2p_k^3p_l^5p_l^6+2p_k^2p_k^5p_l^3p_l^6-2p_k^2p_k^3p_k^5p_k^6\right\}.\end{aligned}\tag{48}$$

The remaining products in (46) can be evaluated similarly resulting in

$$\begin{aligned}E\{c^2c^3c^5c^6\} = E_{\theta,\phi}\Bigg\{&\sum_{k,l}p_k^2p_k^3p_l^5p_l^6+\underline{2p_k^2p_k^5p_l^3p_l^6}\\ &-\underline{2p_k^2p_k^3p_k^5p_k^6}+s_k^2s_k^3s_l^5s_l^6\\ &+\underline{2s_k^2s_k^5s_l^3s_l^6}-\underline{2s_k^2s_k^3s_k^5s_k^6}\\ &+p_k^2p_k^3s_l^5s_l^6+s_k^2s_k^3p_l^5p_l^6\\ &+\underline{4p_k^2p_k^5s_l^3s_l^6}\Bigg\}.\end{aligned}\tag{49}$$

The underlined terms contribute to the XM distortion and the rest contribute to the gain compression or expansion of the jammer. Further on, we will concentrate on the former ones.

The averages of products in (49) can be evaluated directly in a closed form using symbolic math, as was done in [16]. However, in this particular case, the result is very lengthy and difficult to use. Instead, we will recognize that the multiplicands in each product depend only on the corresponding delays (τ_2, τ_3, τ_5, and τ_6) and, therefore, can be individually integrated over these delays with the corresponding exponential terms from (42) as follows:

$$\begin{aligned}\int_{-\infty}^{\infty}&p_k(t-\tau)e^{j\omega\tau}\,d\tau\\ &= \frac{e^{j\omega(Bt+\phi/\pi-k)/B}}{2B}\\ &\quad\cdot\left\{e^{-j[\theta-\omega_c(\phi/\pi-k)/B]}\Pi\left(\frac{\omega_c+\omega}{2\pi B}\right)\right.\\ &\qquad\left.+e^{j[\theta-\omega_c(\phi/\pi-k)/B]}\Pi\left(\frac{\omega_c-\omega}{2\pi B}\right)\right\}\end{aligned}\tag{50a}$$

$$\begin{aligned}\int_{-\infty}^{\infty}&s_k(t-\tau)e^{j\omega\tau}\,d\tau\\ &= j\frac{e^{j\omega(Bt+\phi/\pi-k+1/2)/B}}{2B}\\ &\quad\cdot\left\{e^{-j[\theta-\omega_c(\phi/\pi-k+1/2)/B]}\Pi\left(\frac{\omega_c+\omega}{2\pi B}\right)\right.\\ &\qquad\left.-e^{j[\theta-\omega_c(\phi/\pi-k+1/2)/B]}\Pi\left(\frac{\omega_c-\omega}{2\pi B}\right)\right\}\end{aligned}\tag{50b}$$

where $\Pi(z)$ is the rectangle function [14]. After integration, the multiplicands with the same summation index are multiplied and summed. For example, the product $p_k^2 p_k^5$ of the second and ninth summands in (49) can be evaluated as follows:

$$\begin{aligned}\int_{-\infty}^{\infty} p_k(-\tau_2)e^{j\omega_2\tau_2}\,d\tau_2 \int_{-\infty}^{\infty} p_k(\tau-\tau_5)e^{j\omega_5\tau_5}\,d\tau_5 &= \frac{e^{j(\omega_2+\omega_5)(\phi/\pi-k)/B}e^{j\omega_5\tau}}{(2B)^2} \cdot\Bigg\{e^{-j2[\theta-\omega_c(\phi/\pi-k)/B]}\Pi\left(\frac{\omega_c+\omega_2}{2\pi B}\right)\Pi\left(\frac{\omega_c+\omega_5}{2\pi B}\right) \\ &\quad + e^{j2[\theta-\omega_c(\phi/\pi-k)/B]}\Pi\left(\frac{\omega_c-\omega_2}{2\pi B}\right)\Pi\left(\frac{\omega_c-\omega_5}{2\pi B}\right) \\ &\quad + \Pi\left(\frac{\omega_c+\omega_2}{2\pi B}\right)\Pi\left(\frac{\omega_c-\omega_5}{2\pi B}\right) \\ &\quad + \Pi\left(\frac{\omega_c-\omega_2}{2\pi B}\right)\Pi\left(\frac{\omega_c+\omega_5}{2\pi B}\right)\Bigg\}. \end{aligned} \tag{51}$$

The summation is performed on those multiplicands of the above equation that depend on k. For example, the last two summands in the braces are scaled by $\exp[-jk(\omega_2+\omega_5)/B]$. Recognizing that this quantity is the Fourier transform of a delta function, its infinite sum can be evaluated using the Poisson sum formula

$$\sum_{k=-\infty}^{\infty} e^{-jk(\omega_2+\omega_5)/B} = 2\pi B \sum_{n=-\infty}^{\infty} \delta(\omega_2+\omega_5-2\pi Bn). \tag{52}$$

Using the following identity [14]:

$$\Pi\left(\frac{z-a}{\Delta z}\right)\Pi\left(\frac{z-b}{\Delta z}\right) = \Pi\left(\frac{a-b}{2\Delta z}\right)\Pi\left(\frac{z-(a+b)/2}{\Delta z-|a-b|}\right) \tag{53}$$

it can be shown that the last two summands in (51) are zero outside $(\omega_2+\omega_5-2\pi B,\ \omega_2+\omega_5+2\pi B)$ interval and, therefore, multiplying them by the infinite sum of delta functions in (52) leaves only $\delta(\omega_2+\omega_5)$ in that sum.

After evaluating all underlined products in (49) using the described methodology, they are averaged over θ according to the rule $E_\theta\{\pm jn\theta\} = 0$, where n is an integer. Substituting the evaluated and averaged products of (49) into (42) and keeping only the terms centered around ω_j, we get the following autocorrelation function of the XM distortion:

$$\begin{aligned} R_{\rm XM}(\tau) = \frac{9V_j^2V_{c,\rm rms}^4}{2(2\pi B)^2} &\int_{-\pi B}^{\pi B}\int_{-\pi B}^{\pi B} B_3(\omega_j,\,\omega_c+u,\,-\omega_c-v) \cdot\cos\left[(\omega_j+u-v)\tau\right] \\ &\cdot\Bigg\{B_3(-\omega_j,\,-\omega_c-u,\,\omega_c+v) - \frac{1}{2\pi B} \\ &\quad\cdot\int_{-\pi B}^{\pi B} B_3(-\omega_j,\,-\omega_c-z,\,\omega_c+z-u+v) \\ &\quad\cdot\Pi\left(\frac{z-u+v}{2\pi B}\right)dz\Bigg\}\,du\,dv. \end{aligned} \tag{54}$$

The integral in the braces is due to the correction terms of (49), $-2p_k^2p_k^3p_k^5p_k^6$ and $-2s_k^2s_k^3s_k^5s_k^6$, that distinguish the CDMA signal statistics from those of NBGN.

The PSD function of XM is

$$S_{\rm XM}(\omega) = \int_{-\infty}^{\infty} R_{\rm XM}(\tau)e^{-j\omega\tau}\,d\tau = S_{\rm XM}^{+}(\omega) + S_{\rm XM}^{-}(\omega) \tag{55}$$

where $S_{\rm XM}^{-}(\omega) = S_{\rm XM}^{+}(-\omega)$ and

$$\begin{aligned} S_{\rm XM}^{+}(\omega) = \frac{9V_j^2V_{c,\rm rms}^4}{8\pi B^2}&\int_{-\pi B}^{\pi B} B_3(\omega_j,\,\omega_c+u,\,\omega-\omega_j-\omega_c-u) \cdot\Pi\left(\frac{u+\omega_j-\omega}{2\pi B}\right) \\ &\cdot\Bigg\{B_3(-\omega_j,\,-\omega_c-u,\,-\omega+\omega_j+\omega_c+u) - \frac{1}{2\pi B} \\ &\quad\cdot\int_{-\pi B}^{\pi B} B_3(-\omega_j,\,-\omega_c-z,\,-\omega+\omega_j+\omega_c+z) \\ &\quad\cdot\Pi\left(\frac{z+\omega_j-\omega}{2\pi B}\right)dz\Bigg\}\,du. \end{aligned} \tag{56}$$

B_3 depends on the circuit impedances at the frequency arguments and their linear combinations. Assuming that the circuit impedances are frequency independent within $\pm 2\pi B$ around ω_j, ω_c, $\omega_j-\omega_c$, and $\omega_j+\omega_c$, (56) simplifies to

$$\begin{aligned} S_{\rm XM}^{+}(\omega) = \frac{9V_j^2V_{c,\rm rms}^4}{4B}\,\frac{|\omega-\omega_j|}{2\pi B}\left(1-\frac{|\omega-\omega_j|}{2\pi B}\right) \\ \cdot\left|B_3(\omega_j,\,\omega_c,\,\omega-\omega_j-\omega_c)\right|^2 \end{aligned} \tag{57}$$

for $|\omega-\omega_j| < 2\pi B$. The factor $|\omega-\omega_j|/(2\pi B)$ that is responsible for the XM power drop to zero at $\omega=\omega_j$ comes from the term in the braces of (56). Note that (57) was derived without any assumptions regarding the circuit behavior in the CDMA baseband.

REFERENCES

[1] *Recommended Minimum Performance Standards for cdma2000 Spread Spectrum Mobile Stations*, ANSI/TIA/EIA-98-D Standard, Nov. 2000.

[2] S. Ciccarelli, "Cross modulation and phase noise effects in single-tone desense," QUALCOMM Inc., San Diego, CA, Internal Memo., Sept. 1998.

[3] R. Mohindra, "Cross modulation and linearization in CDMA mobile phone transceivers," in *7th Annu. Wireless Symp./Portable by Design Conf. Dig.*, San Jose, CA, Feb. 22–26, 1999.

[4] A. H. J. N. Van Dijkum and J. J. Sips, "Cross modulation and modulation distortion in A.M. receivers equipped with transistors," *Electron. Applicat.*, vol. 20, no. 3, pp. 107–127, 1959–1960.

[5] D. D. Weiner, K. L. Su, and J. F. Spina, "Reduction of circuit intermodulation distortion via the design of linear out-of-band behavior," presented at the IEEE Electomagnetic Components Symp., Oct. 1975, Paper 6BI.

[6] V. Aparin and C. Persico, "Effect of out-of-band terminations on intermodulation distortion in common-emitter circuits," in *IEEE MTT-S Int. Microwave Symp. Dig.*, vol. 3, June 1999, pp. 977–980.

[7] K. L. Fong, "High-frequency analysis of linearity improvement technique of common-emitter transconductance stages using a low-frequency-trap network," *IEEE J. Solid-State Circuits*, vol. 35, pp. 1249–1171, Aug. 2000.

[8] J. Vuolevi and T. Rahkonen, "The effects of source impedance on the linearity of BJT common-emitter amplifiers," in *Proc. ISCAS*, vol. IV, May 2000, pp. 197–200.

[9] Q. Wu, M. Testa, and R. Larkin, "On design of linear RF power amplifier for CDMA signals," *Int. J. RF Microwave Computer-Aided Eng.*, vol. 8, no. 3, pp. 283–292, 1998.
[10] K. Gard, H. Gutierrez, and M. Steer, "Characterization of spectral regrowth in microwave amplifiers based on the nonlinear transformation of a complex Gaussian process," *IEEE Trans. Microwave Theory Tech.*, vol. 47, pp. 1059–1069, July 1999.
[11] J. B. Thomas, *An Introduction to Statistical Communication Theory*. New York: Wiley, 1969.
[12] M. Schetzen, *The Volterra and Wiener Theories of Nonlinear Systems*. New York: Wiley, 1980.
[13] V. Aparin, B. Butler, and P. Draxler, "Cross modulation distortion in CDMA receivers," in *IEEE MTT-S Int. Microwave Symp. Dig.*, vol. 3, June 2000, pp. 1953–1956.
[14] R. J. Marks, II, *Introduction to Shannon Sampling and Interpolation Theory*. New York: Springer-Verlag, 1991.
[15] D. Borwein and J. M. Borwein, "Some remarkable properties of sinc and related integrals," *The Ramanujan J.*, to be published.
[16] V. Aparin, "Analysis of CDMA signal spectral regrowth and waveform quality," *IEEE Trans. Microwave Theory Tech.*, vol. 49, pp. 2306–2314, Dec. 2001.
[17] K. L. Fong and R. G. Meyer, "High-frequency nonlinearity analysis of common-emitter and differential-pair transconductance stages," *IEEE J. Solid-State Circuits*, vol. 33, pp. 548–555, Apr. 1998.

Vladimir Aparin received the Diploma of Engineer-Physicist degree (with honors) in electronics and automatics from the Moscow Institute of Electronic Engineering (MIEE), Moscow, Russia, in 1989, and is currently working toward the Ph.D. degree in electrical engineering at the University of California at San Diego, La Jolla.

From 1987 to 1992, he was involved in the design and testing of high-speed analog and digital GaAs integrated circuits (ICs) in the device modeling and characterization at the MIEE. From 1992 to 1996, he was with the Hittite Microwave Corporation, where he designed GaAs and Si BiCMOS RF integrated circuits (RFICs) for communication systems. Since 1996, he has been with QUALCOMM Inc., San Diego, CA, where he designs RFIC products for CDMA systems. He has coauthored several technical papers. He holds seven patents.

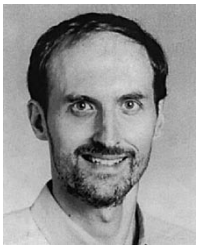

Lawrence E. Larson (S'82–M'86–SM'90–F'00) received the B.S. and M. Eng. degrees in electrical engineering from Cornell University, Ithaca, NY, in 1979 and 1980, respectively, the Ph.D. degree in electrical engineering and MBA degree from the University of California at Los Angeles (UCLA), in 1986 and 1996, respectively.

From 1980 to 1996, he was with Hughes Research Laboratories, Malibu, CA, where he directed the development of high-frequency microelectronics in GaAs, InP, and Si/SiGe and MEMS technologies. In 1996, he joined the faculty of the University of California at San Diego (UCSD), La Jolla, where he is currently the Inaugural Holder of the Communications Industry Chair. He is currently Director of the UCSD Center for Wireless Communications. During the 2000–2001 academic year, he was on leave with IBM Research, San Diego, CA, where he directed the development of RF integrated circuits (RFICs) for third-generation (3G) applications. He has authored or coauthored over 150 papers. He holds 24 U.S. patents.

Dr. Larson was the recipient of the 1995 Hughes Electronics Sector Patent Award for his work on RF MEMS technology. He was corecipient of the 1996 Lawrence A. Hyland Patent Award of Hughes Electronics for his work on low-noise millimeter-wave high electron-mobility transistors (HEMTs), and the 1999 IBM Microelectronics Excellence Award for his work in Si/SiGe HBT technology.